Report

Current Biology

A Putative Mechanism for Magnetoreception by Electromagnetic Induction in the Pigeon Inner Ear

Graphical Abstract

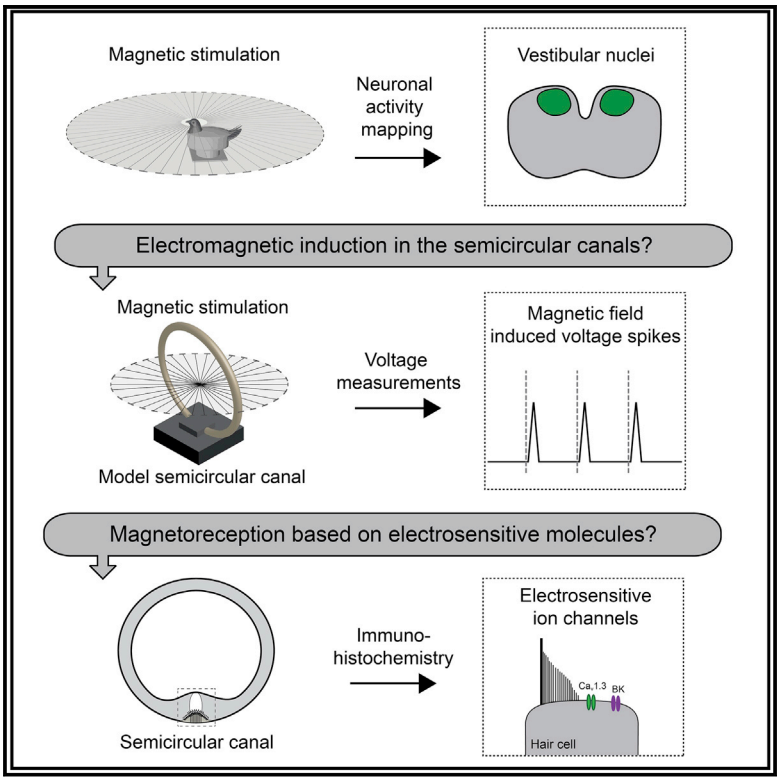

Highlights

- Magnetic stimuli activate neurons in the caudal vestibular nuclei
- Magnetic stimuli induce a voltage in a model of a semicircular canal
- Electroreceptive molecules are expressed in vestibular hair cells
- We postulate that pigeons detect magnetic fields by electromagnetic induction

Authors

Simon Nimpf,
Gregory Charles Nordmann,
Daniel Kagerbauer, ...,
Martin Colombini, Matthew J. Mason,
David Anthony Keays

Correspondence

keays@imp.ac.at

In Brief

Nimpf, Nordmann et al. confirm that magnetic stimuli result in neuronal activity in the vestibular nuclei of pigeons. Hypothesizing that this is attributable to electromagnetic induction within semicircular canals of the inner ear, they demonstrate the presence of known electrosensory molecules in vestibular hair cells.

Nimpf et al., 2019, Current Biology 29, 4052–4059
December 2, 2019
https://doi.org/10.1016/j.cub.2019.09.048

CellPress

CellPress

Current Biology
Report

A Putative Mechanism for Magnetoreception by Electromagnetic Induction in the Pigeon Inner Ear

Simon Nimpf,[1,5] Gregory Charles Nordmann,[1,5] Daniel Kagerbauer,[2] Erich Pascal Malkemper,[1] Lukas Landler,[1] Artemis Papadaki-Anastasopoulou,[1] Lyubov Ushakova,[1] Andrea Wenninger-Weinzierl,[1] Maria Novatchkova,[1] Peter Vincent,[3] Thomas Lendl,[1] Martin Colombini,[1] Matthew J. Mason,[4] and David Anthony Keays[1,6,*]

[1]Research Institute of Molecular Pathology (IMP), Vienna Biocenter (VBC), Campus-Vienna-Biocenter 1, 1030 Vienna, Austria
[2]Atominstitut, TU Wien, Stadionallee 2, 1020 Vienna, Austria
[3]Department of Neurology, Yale University School of Medicine, 333 Cedar Street, New Haven, CT 06520, USA
[4]Department of Physiology, Development and Neuroscience, University of Cambridge, Downing Street, Cambridge CB2 3EG, UK
[5]These authors contributed equally
[6]Lead Contact
*Correspondence: keays@imp.ac.at
https://doi.org/10.1016/j.cub.2019.09.048

SUMMARY

A diverse array of vertebrate species employs the Earth's magnetic field to assist navigation. Despite compelling behavioral evidence that a magnetic sense exists, the location of the primary sensory cells and the underlying molecular mechanisms remain unknown [1]. To date, most research has focused on a light-dependent radical-pair-based concept and a system that is proposed to rely on biogenic magnetite (Fe_3O_4) [2, 3]. Here, we explore an overlooked hypothesis that predicts that animals detect magnetic fields by electromagnetic induction within the semicircular canals of the inner ear [4]. Employing an assay that relies on the neuronal activity marker C-FOS, we confirm that magnetic exposure results in activation of the caudal vestibular nuclei in pigeons that is independent of light [5]. We show experimentally and by physical calculations that magnetic stimulation can induce electric fields in the pigeon semicircular canals that are within the physiological range of known electroreceptive systems. Drawing on this finding, we report the presence of a splice isoform of a voltage-gated calcium channel ($Ca_V1.3$) in the pigeon inner ear that has been shown to mediate electroreception in skates and sharks [6]. We propose that pigeons detect magnetic fields by electromagnetic induction within the semicircular canals that is dependent on the presence of apically located voltage-gated cation channels in a population of electrosensory hair cells.

RESULTS

Magnetically Induced Activation in the Pigeon Vestibular Brainstem

We set out to replicate a previous study conducted by Wu and Dickman, who reported that magnetic stimuli induce neuronal activation in the vestibular nuclei of pigeons [5]. To perform this experiment within the laboratory environment, we built a room constructed of mu metal surrounded by an aluminum Faraday cage to shield against static and oscillating magnetic fields (Figure 1A). This setup allowed us to perform experiments in a controlled, magnetically clean environment [7]. Magnetic fields were generated using a double-wrapped, custom-built 3D Helmholtz coil system situated in the center of the shielded room (Figure 1B). To reduce movement during the experiments, birds were head fixed using a surgically implanted plastic head post, and the body was immobilized using a 3D printed harness (Figure 1C). We applied the same stimulus as Wu and Dickman, exposing adult pigeons to a 150-μT, rotating magnetic field (n = 22) or to a zero magnetic field (n = 23) for 72 min (Figures 1D–1F) [5]. We performed this experiment both in darkness (n = 30) and under broad-spectrum white light (n = 15). Birds were then perfused, the brains were sliced, and matched sections containing the vestibular nuclei (3 sections per bird) were stained with sera against the neuronal activity marker C-FOS. To minimize variation, all staining was performed simultaneously, all slides were scanned with the same exposure settings, and C-FOS-positive neurons were counted using a machine-learning-based algorithm. Using established anatomical coordinates, we segmented the medial vestibular nuclei (VeM) and compared the density of C-FOS-positive cells of the experimental groups [8]. We observed an increase in the density of C-FOS-positive cells in both the light and dark when exposing birds to magnetic fields. In the light, the average density in controls was 35.32 ± 10.20 cells/mm^2 (n = 8; mean ± SD) whereas with the magnetic treatment it was 44.38 ± 5.72 cells/mm^2 (n = 7; mean ± SD). In the dark, the average density for control birds was 34.70 ± 10.82 cells/mm^2 (n = 15; mean ± SD) whereas with the magnetic treatment it was 50.52 ± 27.34 cells/mm^2 (n = 15; mean ± SD). An application of a two-way ANOVA revealed a significant effect of the magnetic treatment but no interaction between magnetic treatment and lighting conditions (two-way ANOVA; magnetic: $p = 0.0176$, $F = 6.125$; magnetic by light: $p = 0.5675$, $F = 0.332$) (Figures 2A and 2B; Table S1). To explore this in more detail, we employed our spot-detection algorithm coupled to an elastic registration to generate heatmaps showing regional

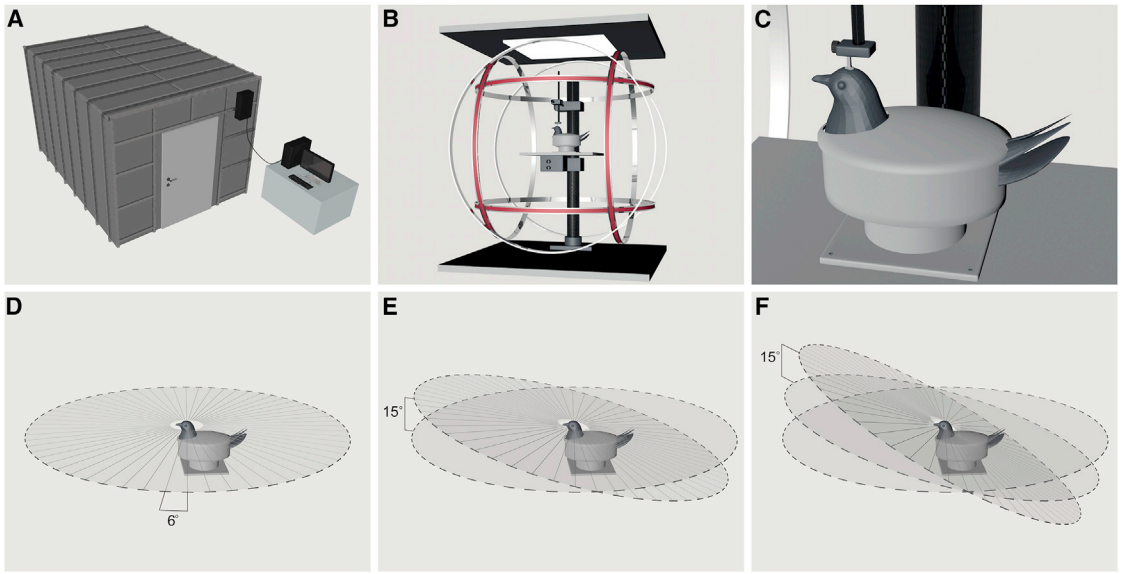

Figure 1. Experimental Setup for the Magnetic Activation Study

(A) The magnetic activation experiments were performed inside a magnetically shielded room consisting of a Faraday cage to shield from broadband anthropogenic magnetic noise and a mu-metal cage to shield from the geomagnetic field.

(B and C) Pigeons were placed in the center of a double-wrapped 3D Helmholtz coil system (B) located in the magnetically shielded room and immobilized by head fixation and a molded body harness (C).

(D–F) Schematic illustration of the magnetic stimulus used in this study. The magnetic field vector was rotated 360° within a plane by 6° steps every 2 s (D). After each rotation the plane was shifted by 15° (E) and the procedure was repeated until a full rotation around each axis was achieved (12 planes per x, y, and z axis, respectively) (F).

differences in the density of C-FOS-positive cells. This revealed an enrichment of activated neurons in the dorsomedial part of the VeM in animals exposed to magnetic stimuli (Figure 2C). Previous tracing experiments have shown that the dorsomedial VeM is innervated by projections from both the semicircular canals and the otolith organs located in the inner ear [9].

A Model for Electromagnetic Induction in the Pigeon Inner Ear

As we did not observe an interaction between the presence of light and magnetically induced neuronal activation, our results are consistent with a magnetic sensory system based on either magnetite or electromagnetic induction [10]. We have previously reported the discovery of an iron-rich organelle in both vestibular and cochlear hair cells that is associated with vesicular structures, but because it is primarily composed of ferrihydrite it lacks the magnetic properties to function as the hypothesized torque-based magnetoreceptor [11–13]. Moreover, a systematic screen for magnetite in the pigeon lagena using synchrotron-based X-ray fluorescence microscopy and electron microscopy has failed to identify extra- or intracellular magnetite crystals [14]. In light of these findings, we focused on electromagnetic induction [15]. First proposed by Camille Viguier in 1882, this hypothesis predicts that as a terrestrial animal moves through the Earth's static magnetic field a voltage is induced within the conductive endolymph of the semicircular canals [4, 16].

To test the viability of this hypothesis, we built a simple model of a pigeon semicircular canal by filling a plastic tube with artificial pigeon endolymph (see STAR Methods; Figure 3A) [17]. The tubing was closed on both sides with electrodes connected to a nanovoltmeter (forming a loop with a diameter of 21 cm), placed in the center of our magnetic coil system, and exposed to the same rotating magnetic stimulus applied to our birds (i.e., 150 μT rotating 360° with 6°-step changes every 2 s). We observed discrete voltage spikes when the magnetic field stimulus was presented and with each stepwise change (Figure 3B). In accordance with Faraday's law of electromagnetic induction, we observed the maximum induced voltage (15.6 μV) when the magnetic field vector was perpendicular (90°) to the plane of the canal and lowest (1.6 μV) when the vector was parallel to the plane of the canal (0°) (Figure 3B). In contrast, when presenting the control stimulus (with the current running antiparallel through the double-wrapped coils), we did not observe these characteristic voltage spikes (Figure 3C). Nor did we observe voltage spikes when removing the model of the semicircular canal from the circuit, demonstrating that induction does not occur in the connecting shielded wires (Figure 3D).

Next, we measured the dimensions of the semicircular canals in pigeons drawing on previously generated computed tomography (CT) scans (n = 3 birds) [18] (Figure S1A). This revealed that the mean loop diameter of the posterior canal was 4.20 ± 0.01 mm, the anterior canal was 6.37 ± 0.05 mm, and the lateral canal was 5.18 ± 0.15 mm (mean ± SD). Drawing on these measurements and the voltage induced in our 21-cm-diameter model, we were able to estimate the electric field generated within a pigeon's semicircular canal on presentation of the Wu and Dickman stimulus. We applied the following equation: $E = (u/2\pi r)$, where E is the electric field, r is the mean radius of the semicircular canal loop, and u is the measured induced voltage. This revealed a maximal electric field in the anterior

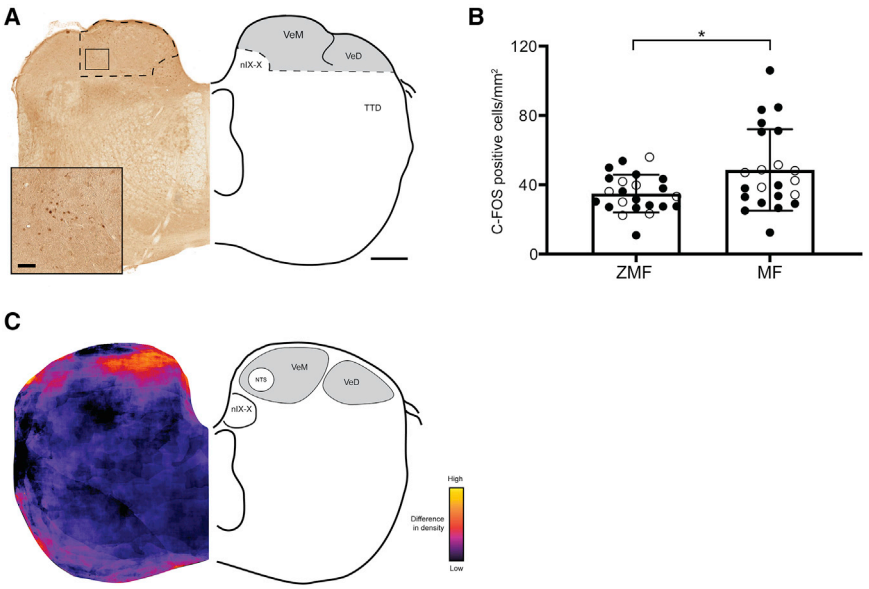

Figure 2. Magnetically Induced Neuronal Activation in the Pigeon Vestibular Nuclei

(A) Representative coronal section stained with sera that bind to the neuronal activity marker C-FOS. Dark-stained nuclei are visible in the inset. Adjacent schematic representation of the pigeon brainstem shows the medial and descending vestibular nuclei (VeM and VeD) in gray [8].

(B) Quantification of C-FOS-positive cells per mm^2 in VeM in birds that were exposed to a rotating magnetic field (MF; n = 22) and to a zero magnetic field control (ZMF; n = 23) (two-way ANOVA; p = 0.0176, F = 6.125). Filled and open circles represent animals that were tested in the dark (n = 15 for ZMF andMF) and in light (n = 8 for ZMF and n = 7 for MF), respectively.

(C) Heatmap showing the regional difference in C-FOS cell density in the vestibular nuclei when comparing the MF and ZMF groups. Magnetically responsive neurons were enriched in the dorsomedial region of the VeM.

Data are presented as mean ± SD. *p < 0.05. Scale bars represent 500 μm (A) and 50 μm (A, inset). VeM, vestibular nucleus medialis; VeD, vestibular nucleus descendens; TTD, nucleus et tractus descendens nervi trigemini; NTS, nucleus tractus solitarius; nIX-X, nucleus nervi glossopharyngei et nucleus motorius dorsalis nervi vagi. See also Table S1.

canal of 7.2 nV/cm, 5.8 nV/cm for the lateral canal, and 4.7 nV/cm for the posterior canal when applying a rotating 150-μT stimulus. We repeated the aforementioned experiment, applying a 50-μT stimulus, again rotating 360° in 2 min with 6°-step changes every 2 s. This revealed a maximal electric field in the anterior canal of 2 nV/cm, 1.6 nV/cm for the lateral canal, and 1.3 nV/cm for the posterior canal (Figures S1B–S1D).

In our experiment, we applied a changing magnetic stimulus to a bird that is head fixed; however, in the natural environment, we imagine that pigeons employ head scanning to alter the orientation of their semicircular canals with respect to the magnetic vector. To assess whether this natural behavior would be sufficient to induce electric fields that are physiologically relevant, we estimated the electric field generated using the following equation, which is derived from Maxwell's third law: $E_n = B_0 \cdot \pi f \cdot r$, where r is the radius of the semicircular canals, B_0 is the Earth's field, and f is the frequency of head scanning [19]. It has recently been shown that pigeons undertake head scanning during flight that exceeds 700°/s [20]. Based on this frequency and the radii of the semicircular canals reported here, we estimate that natural head movement will generate electric fields in the range of 7.9–9.6 nV/cm in an Earth-strength field (50 μT). Because previous studies have shown that electrosensitive animals can detect fields as small as 5 nV/cm [21, 22], we conclude that the Wu and Dickman stimulus and natural head-scanning behavior could induce voltages within the semicircular canals that are within the detectable range of known electrosensory systems.

Electroreceptive Molecules Are Expressed in the Pigeon Inner Ear

If magnetoreception in pigeons relies on the conversion of magnetic fields into an electric signal, the magnetosensory apparatus might resemble known electroreceptive epithelia on a cellular and molecular level. Ampullae of Lorenzini are electrosensory organs found in cartilaginous fish that consist of specialized sensory cells located at the base of gel-filled canals [22]. Recent work in little skate (*Leucoraja erinacea*) has shown that the voltage-sensitive calcium channel $Ca_V1.3$/CACNA1D and the large-conductance calcium-activated potassium channel BK/KCNMA1 are enriched in these cells and facilitate electrosensation [23]. Given the ontogenetic proximity of electrosensory, auditory, and vestibular hair cells, we asked whether these electrosensory molecules are present in the pigeon semicircular canals [24]. To function as electroreceptors, we would expect these channels to be apically located in hair cells where they would be exposed to the endolymph (Figures 4A–4C). To test this prediction, we performed fluorescence immunohistochemistry on pigeon ampullary hair cells (n = 3 birds). Staining with sera against the BK channel revealed an enrichment of apical staining in hair cells that are positive for the marker otoferlin (Figures 4D, 4F, 4G, and S2D–S2I) [25, 26]. Consistent with previous studies, we observed goblet-shaped $Ca_V1.3$ staining at hair cell ribbon synapses [27] and a punctate enrichment at the apical membrane that has not previously been reported (Figures 4E and 4G). High-resolution confocal imaging further revealed that these $Ca_V1.3$-rich plaques are most pronounced at the base of the kinocilium, and that $Ca_V1.3$ is localized in the kinocilium itself (Figures S2A–S2C).

In sharks and skates, $Ca_V1.3$ is characterized by a low threshold of activation attributable to a 10-amino acid lysine-rich insertion located in the intracellular loop between IVS2 and IVS3 of the alpha subunit (Figure 4H). It has been shown that mutating the charged lysine residues in this insertion to neutral glutamine residues results in a channel with a higher threshold for activation [6, 23]. Interestingly, Hudspeth and colleagues have reported a similar insertion in $Ca_V1.3$ that is expressed in the hair cells of chickens [28]. To ascertain whether this charged insertion is expressed in pigeons, we drew on the available

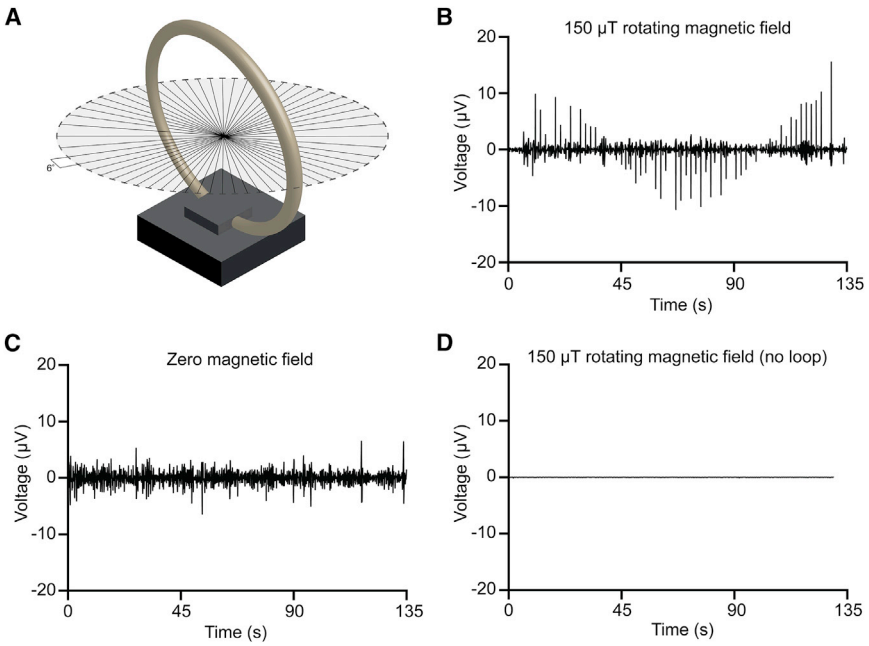

Figure 3. Modeling of Electromagnetic Induction in the Pigeon Inner Ear

(A) A model of a pigeon semicircular canal (21 cm in diameter) containing artificial endolymph was exposed to a 150 μT rotating magnetic field. The stimulus consisted of 6° shifts every 2 s, completing one rotation in 2 min around the vertical axis. The induced voltage was measured using a nanovoltmeter.

(B) We observed voltage spikes correlating with changes in the magnetic field. The peak amplitude was highest (15.6 μV) when the stimulus was directed 90° to the plane of the canal and lowest (1.6 μV) when the vector was parallel to the plane of the canal.

(C) These voltage spikes were absent when the control stimulus was presented with currents running antiparallel through the double-wrapped coils.

(D) Voltage spikes were likewise absent when the 150 μT rotating magnetic field was exposed to a circuit that did not include the loop containing the artificial endolymph. This shows that induction does not occur in the connecting wires.

See also Figure S1.

genomic resources, determined the gene structure, and designed a PCR-based strategy with primers flanking the putative insertion site (Figures 4H and S3A) [29]. We extracted mRNA and generated cDNA libraries for a broad range of tissues from the pigeon including brain, spleen, muscle, retina, basilar papilla, vestibular epithelia, skin, and heart (n = 3 birds). Analysis by gel electrophoresis showed that $Ca_V1.3$ is absent in the respiratory concha, muscle, and liver but is otherwise broadly expressed. Strikingly, we only observed PCR products consistent with a larger splice isoform in the cochlea and vestibular system (Figure 4I). Cloning of these PCR products revealed an insertion of 10 amino acids rich in lysine residues with notable homology to that reported in sharks and skates (Figure 4J). We refer to this variant as the KKER splice isoform.

In skates it has been shown that $Ca_V1.3$ works in conjunction with the BK potassium channel, which has a unique conductance profile due to the expression of an alternatively spliced exon [23]. This variant is distinguished by the presence of an arginine residue at position 340 (R340) and an alanine residue at 347 (A347), which are located intracellularly near the pore of the channel (Figure 4K). We refer to this variant as the RA splice isoform. To ascertain whether this splice isoform is expressed in pigeons, we first determined the genetic architecture of pigeon KCNMA1 (Figure S3B). Drawing on this information, we designed a PCR-based assay that relies on the amplification of exon 9a/b from cDNA libraries, followed by digestion with the restriction enzyme AluI (Figures 4L and S3B). In the event the RA isoform is amplified (exon 9b), the amplicon is resistant to AluI digestion, resulting in the presence of a larger band (239 bp). We found that KCNMA1 is broadly expressed in the pigeon; however, the RA isoform was enriched in the retina and vestibular system. We conclude that the molecular apparatus necessary for the detection of small electric fields is present within the pigeon vestibular apparatus.

Phylogenetic Analysis of $Ca_V1.3$/CACNA1D and BK/KCNMA1

Finally, we explored the phylogenetic distribution of the splice isoforms of CACNA1D and KCNMA1 among Animalia. To identify CACNA1D homologs containing the long KKER splice isoform, we performed a BLASTp search with a 50-amino-acid-long segment of pigeon $Ca_V1.3$, centered around the splice isoform. We found that this insertion first emerged in Gnathostomata and has a limited distribution. It is found in skates, sharks, bats, turtles, rainbow trout, and birds (Figures 4I and S4A). In the case of the KCNMA1 RA isoform, a BLASTp search revealed that it is present in numerous animals including skates, electric eels, numerous fish and many bird species, rodents (including *Mus musculus*), primates (including *Homo sapiens*), bats, dolphins, and whales (Figures 4L and S4B). We conclude that the RA splice isoform of KCNMA1 is widely distributed in vertebrates whereas the KKER isoform of CACNA1D is often found in phyla that are known to possess an electric or magnetic sense.

DISCUSSION

In 1882, Viguier speculated that "the geomagnetic field determines, within the endolymph of the canals, induced currents, whose intensities vary dependently of both the canals' positions in relation to inclination and declination, and the intensity of the magnetic field" [4]. In this manuscript, we have explored this hypothesis, one that has largely been ignored by the scientific community since its proposition. We present data that replicates the work of Wu and Dickman, demonstrating magnetically induced neuronal activation in the vestibular nuclei that is not dependent on light. We show that changing low-intensity magnetic stimuli (150 μT) can induce electric fields that lie within the window of physiological detection and that the molecular machinery necessary to detect such fields is present in the pigeon inner ear. Our data are consistent with a model whereby pigeons detect

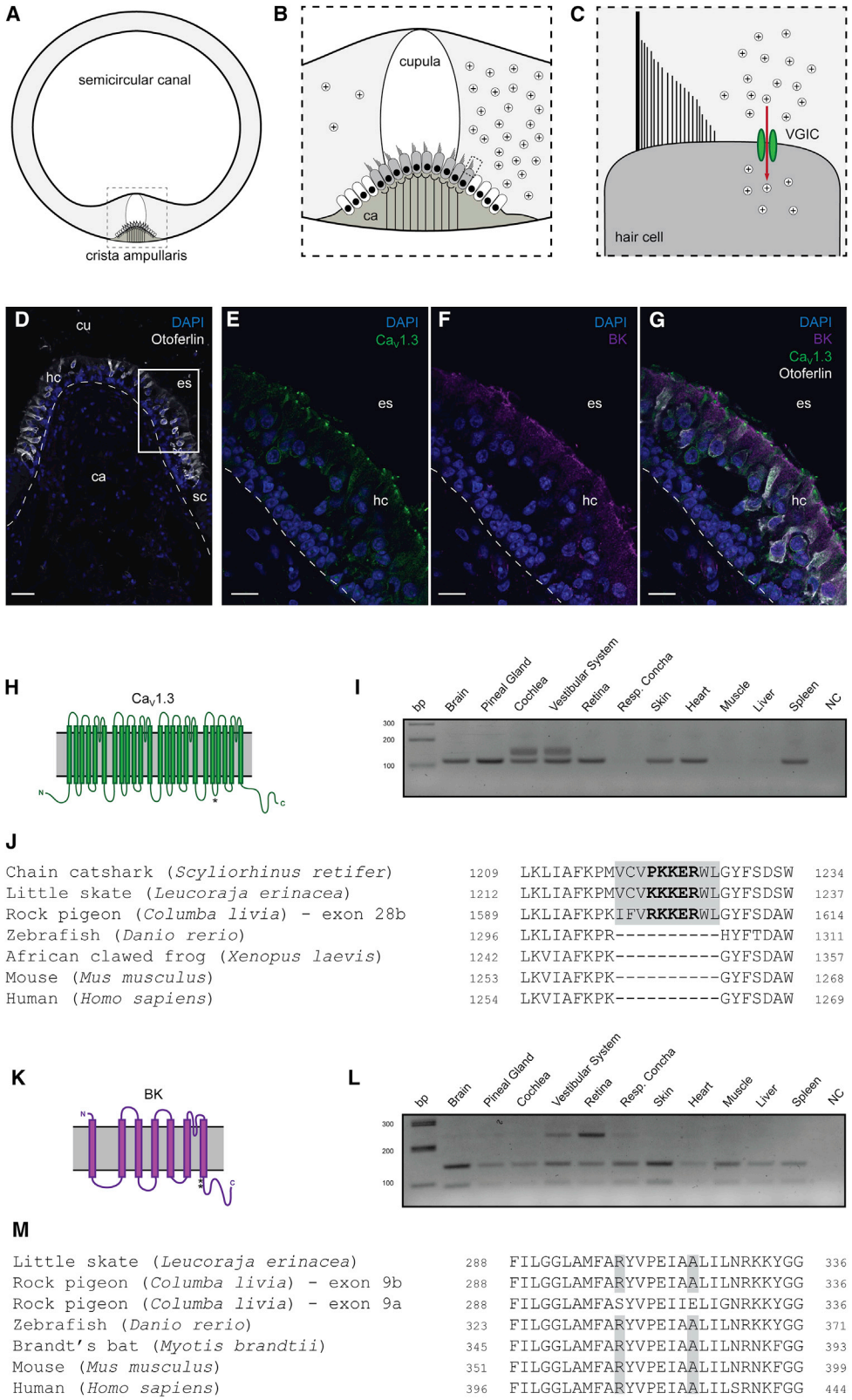

Figure 4. Electroreceptive Molecules Are Expressed in the Pigeon Inner Ear

(A–C) Schematic illustrating induction-based magnetoreception in the pigeon inner ear.

(A) A semicircular canal with sensory hair cells located at the base of the gelatinous cupula at the crista ampullaris (ca).

(legend continued on next page)

magnetic fields by electromagnetic induction within the semicircular canals relying on the presence of apically located voltage-gated calcium channels in a population of electrosensory hair cells.

We have replicated the study of Wu and Dickman with only minor changes to their experimental protocol [5]. Specifically, we employed double-wrapped coils to control for heat and vibration when delivering the magnetic stimuli and a plastic head post and glue in preference to metal screws to head fix the bird and conducted the experiment in both darkness and light. We have further been able to refine the region activated by magnetic stimuli by elastic registration and mapping of C-FOS-positive cells to the dorsomedial part of the VeM. Our results, coupled with the initial study, support the contention that the vestibular system is involved in processing magnetic information in the absence of light. Wu and Dickman had argued that the primary sensors likely reside in the lagena, because extirpation of the cochlear duct abolished magnetically induced activity in the vestibular nuclei. These results, however, are also consistent with magnetosensation by electromagnetic induction, because removal of the cochlear duct would compromise the integrity of the entire endolymphatic system and its ionic constituents.

Magnetosensation by induction has only been considered viable in elasmobranch fish, because surface-electrosensitive epithelia could detect voltages induced as the animal moves through the conductive seawater within the Earth's static magnetic field [21, 22]. In birds, induction has largely been dismissed due to the high electrical resistivity of the air and the lack of a conductive circuit [1]. Our physical modeling and anatomical measurements suggest that the semicircular canals possess the requisite dimensions and properties to function as a physiological dynamo. Moreover, the apical location and the expression of splice isoforms of $Ca_V1.3$/CACNA1D and BK/KCNMA1 indicate that hair cells in pigeons may also function as electroreceptors. It is known that hair cells are closely related to electrosensory cells on a developmental, cellular, and molecular level [24]. The ancestral lateral line system of vertebrates consists of both mechanosensory hair cells and electrosensory ampullary organs, which develop from lateral line embryonic placodes [30]. Both cell types have apical ciliary protrusions and similar gene expression profiles, and share characteristic ribbon synapses [31, 32]. It is therefore conceivable that hair cells in *Aves* have maintained or acquired an electrosensory capacity that is exploited for magnetic detection.

A critical issue in considering the validity of the inductive hypothesis is how magnetic information would be distinguished from vestibular input assuming that ampullary hair cells are both mechanically and electrically sensitive [4, 16]. The anatomical framework of the semicircular canals provides an elegant solution to this problem. Imagine a magnetic vector with an orientation that is perpendicular to the plane of a semicircular canal. Rotation in the plane of the canal leads to inertia-based fluid displacement and mechanic stimulation of hair cells but minimal electromagnetic induction. In contrast, rotation perpendicular to the plane does not result in fluid movement but generates electric field changes [16]. In this way, magnetic and vestibular information originating from the same sensory epithelia could be distinguished from each other, so long as the animal has a third reference frame (e.g., visual input). A second important element to this model is the presence of the cupula within the crista ampullaris. Acting as a physical barrier it enables the separation of positively charged cations (Na^+, K^+) as the animal moves its head through the magnetic field [16]. The permeability of this structure to cations has yet to be determined, but we assume that its gelatinous composition and its positive charge impede cation flow [33, 34].

An experimental paradigm that permits investigators to distinguish between magnetoreception based on induction and magnetite is to fix a strong magnet (e.g., 10 mT) to the bird. Such a field would immobilize any magnetite chains, rendering them unresponsive to the application of an Earth-strength field. In contrast, even a small magnetic vector superimposed onto a larger fixed field would result in a changing magnetic stimulus and permit magnetoreception by electromagnetic induction. Although this experiment has yet to be performed in a controlled laboratory-based assay in pigeons, a number of groups have attached magnets to birds to assess their effect on homing and navigation. Keeton glued bar magnets onto the backs of pigeons, initially reporting that this interfered with their homeward orientation on overcast but not sunny days [35], which was

(B) Rotation of the bird's head perpendicular to the plane of the semicircular canal causes a redistribution of charges across the cupula (cu).
(C) Voltage-gated ion channels (VGIC) that are located apically in hair cells respond to this redistribution of charge, by either allowing or restricting cation influx into the hair cell.
(D) Histological section of a pigeon crista ampullaris stained with the hair cell (hc) marker otoferlin and nuclear marker DAPI (n = 3 birds).
(E–G) Co-staining with $Ca_V1.3$ (E and G) and the large-conductance calcium-activated potassium channel BK (F and G) shows that the voltage-sensitive machinery is expressed in otoferlin-positive hair cells (D and G) and localizes to the apical surface facing the endolymphatic space (es). Note the distinctive apical punctate staining of $Ca_V1.3$.
(H) Schematic representation of a pigeon $Ca_V1.3$ alpha subunit. The IVS2-S3 domain (shown with an asterisk) is encoded by exon 28 and is subject to alternative splicing.
(I) PCR amplification of various cDNA libraries employing primers that flank exon 28. $Ca_V1.3$ is broadly expressed in the pigeon, but the larger splice isoform that encompasses exon 28b is only expressed in the cochlea and vestibular epithelia.
(J) Homology alignment of pigeon $Ca_V1.3$ shows that this long isoform is characterized by charged residues (KKER), which confer a low activation threshold in skates and sharks. This insertion is absent in zebrafish, *Xenopus*, mice, and humans.
(K) Schematic representation of a pigeon BK channel alpha subunit. The domain proximal to the pore is encoded by exon 9 and highlighted with an asterisk.
(L) Gel image of an AluI restriction digest following PCR amplification of cDNA libraries with primers spanning exon 9. Amplicons that include exon 9b contain the RA allele, which is resistant to digestion by AluI, resulting in a single 239-bp band. In contrast, amplicons that encompass exon 9a result in a digestible product that generates two bands (92 and 147 bp). Exon 9a is expressed in all tissues whereas exon 9b (i.e., the RA isoform) is enriched in the vestibular system and the retina.
(M) Homology alignment showing that the RA isoform is also found in zebrafish, bats, mice, and humans.
Scale bars represent 50 μm (D) and 10 μm (E–G). NC, negative control. See also Figures S2–S4.

replicated by Ioalè [36]. However, it should be noted that Keeton himself generated contradictory results when performing a larger study between 1971 and 1979 [37]. Several groups have attached magnets to the heads of albatrosses and observed no effect on navigation, leading the authors to speculate that the birds do not have a magnetite-based magnetosensor, or that they do not rely on magnetic cues for orientation [38, 39]. Although these studies have largely ignored the possibility that birds might rely on electromagnetic induction as a mechanism, we would urge caution when interpreting their results. There are numerous uncontrolled environmental variables, and it is unclear whether the magnets were truly fixed in position given they were glued to the skin of the birds.

Finally, we wish to acknowledge that there are alternative explanations for our results. First, it is conceivable that the magnetically induced activation that we observe in the VeM is a consequence of multimodal sensory integration and not due to primary sensors located in the inner ear. Second, we have assumed that the light-independent magnetic activation we report excludes a radical-pair-based mechanism; however, it is possible that a chemical-based compass may exist and does not depend on light. Moreover, our results do not preclude the existence of a light-based magnetoreceptor in pigeons, because they may possess more than one magnetosensory system. Third, the long isoform of $Ca_V1.3$ (although critical for electroreception in sharks and skates) may merely tune hair cells to auditory and vestibular stimuli in birds. Despite these caveats, the putative mechanism that we present in this paper enables us to make several predictions. Should pigeons rely on $Ca_V1.3$ to detect magnetic fields by electromagnetic induction, we expect that magnetically induced neuronal activation will be compromised by (1) pharmacological intervention with $Ca_V1.3$ antagonists such as nifedipine; (2) hair cell ablation with antibiotics; and (3) genetic deletion of the long isoform of $Ca_V1.3$. In contrast, neuronal activation will be preserved if a strong dipole magnet is fixed on the head of the animal, immobilizing any magnetite particles but still permitting induction from an applied changing stimulus. These predictions will serve as a basis for future experiments and the interrogation of a hypothesis that has been forgotten but not yet falsified.

STAR★METHODS

Detailed methods are provided in the online version of this paper and include the following:

SUPPLEMENTAL INFORMATION

Supplemental Information can be found online at https://doi.org/10.1016/j.cub.2019.09.048.

ACKNOWLEDGMENTS

D.A.K. is supported by the European Research Council (ERC; 336725) and the FWF (Y726). S.N. is a recipient of a DOC fellowship of the Austrian Academy of Sciences at the Research Institute of Molecular Pathology. We wish to thank Boehringer Ingelheim, which funds basic scientific research at the Research Institute of Molecular Pathology. We are indebted to the excellent support facilities at the IMP and VBCF including histology, bio-optics, bioinformatics, and the workshop.

AUTHOR CONTRIBUTIONS

Conceptualization, S.N., G.C.N., and D.A.K.; Investigation, S.N., G.C.N., D.K., E.P.M., L.L., A.P.-A., L.U., A.W.-W., and P.V.; Formal Analysis, S.N., G.C.N., D.K., E.P.M., M.N., and L.L.; Software, T.L.; Resources, M.J.M. and M.C.; Writing – Original Draft, S.N., G.C.N., and D.A.K.; Writing – Review & Editing, E.P.M., M.J.M., P.V., D.K., and L.L.; Funding Acquisition, D.A.K. and S.N.; Supervision, D.A.K.

DECLARATION OF INTERESTS

The authors declare no competing interests.

Received: June 26, 2019
Revised: August 28, 2019
Accepted: September 19, 2019
Published: November 14, 2019

REFERENCES

1. Johnsen, S., and Lohmann, K.J. (2005). The physics and neurobiology of magnetoreception. Nat. Rev. Neurosci. *6*, 703–712.
2. Ritz, T., Adem, S., and Schulten, K. (2000). A model for photoreceptor-based magnetoreception in birds. Biophys. J. *78*, 707–718.
3. Kirschvink, J.L., Walker, M.M., and Diebel, C.E. (2001). Magnetite-based magnetoreception. Curr. Opin. Neurobiol. *11*, 462–467.
4. Viguier, C. (1882). Le sens de l'orientation et ses organes chez les animaux et chez l'homme. Rev. Philos. France Let, 1–36.
5. Wu, L.Q., and Dickman, J.D. (2011). Magnetoreception in an avian brain in part mediated by inner ear lagena. Curr. Biol. *21*, 418–423.
6. Bellono, N.W., Leitch, D.B., and Julius, D. (2018). Molecular tuning of electroreception in sharks and skates. Nature *558*, 122–126.
7. Landler, L., Nimpf, S., Hochstoeger, T., Nordmann, G.C., Papadaki-Anastasopoulou, A., and Keays, D.A. (2018). Comment on "Magnetosensitive neurons mediate geomagnetic orientation in *Caenorhabditis elegans*." eLife *7*, e30187.
8. Karten, H.J., and Hodos, W. (1967). A Stereotaxic Atlas of the Brain of the Pigeon (*Columba livia*) (The Johns Hopkins Press).
9. Dickman, J.D., and Fang, Q. (1996). Differential central projections of vestibular afferents in pigeons. J. Comp. Neurol. *367*, 110–131.
10. Nordmann, G.C., Hochstoeger, T., and Keays, D.A. (2017). Magnetoreception—a sense without a receptor. PLoS Biol. *15*, e2003234.

11. Lauwers, M., Pichler, P., Edelman, N.B., Resch, G.P., Ushakova, L., Salzer, M.C., Heyers, D., Saunders, M., Shaw, J., and Keays, D.A. (2013). An iron-rich organelle in the cuticular plate of avian hair cells. Curr. Biol. *23*, 924–929.
12. Nimpf, S., Malkemper, E.P., Lauwers, M., Ushakova, L., Nordmann, G., Wenninger-Weinzierl, A., Burkard, T.R., Jacob, S., Heuser, T., Resch, G.P., and Keays, D.A. (2017). Subcellular analysis of pigeon hair cells implicates vesicular trafficking in cuticulosome formation and maintenance. eLife *6*, e29959.
13. Jandacka, P., Burda, H., and Pistora, J. (2015). Magnetically induced behaviour of ferritin corpuscles in avian ears: can cuticulosomes function as magnetosomes? J. R. Soc. Interface *12*, 20141087.
14. Malkemper, E.P., Kagerbauer, D., Ushakova, L., Nimpf, S., Pichler, P., Treiber, C.D., de Jonge, M., Shaw, J., and Keays, D.A. (2019). No evidence for a magnetite-based magnetoreceptor in the lagena of pigeons. Curr. Biol. *29*, R14–R15.
15. Faraday, M. (1832). V. Experimental researches in electricity. Philos. Trans. R. Soc. Lond. *122*, 125–162.
16. Jungerman, R.L., and Rosenblum, B. (1980). Magnetic induction for the sensing of magnetic fields by animals—an analysis. J. Theor. Biol. *87*, 25–32.
17. Sauer, G., Richter, C.-P., and Klinke, R. (1999). Sodium, potassium, chloride and calcium concentrations measured in pigeon perilymph and endolymph. Hear. Res. *129*, 1–6.
18. Malkemper, E.P., Mason, M.J., Kagerbauer, D., Nimpf, S., and Keays, D.A. (2018). Ectopic otoconial formation in the lagena of the pigeon inner ear. Biol. Open *7*, bio034462.
19. Feynman, R.P., Leighton, R.B., and Sands, M. (2011). The Feynman Lectures on Physics, Vol. II: The New Millennium Edition: Mainly Electromagnetism and Matter (Basic Books).
20. Kano, F., Walker, J., Sasaki, T., and Biro, D. (2018). Head-mounted sensors reveal visual attention of free-flying homing pigeons. J. Exp. Biol. *221*, jeb183475.
21. Kalmijn, A.J. (1982). Electric and magnetic field detection in elasmobranch fishes. Science *218*, 916–918.
22. Kalmijn, A.J. (1971). The electric sense of sharks and rays. J. Exp. Biol. *55*, 371–383.
23. Bellono, N.W., Leitch, D.B., and Julius, D. (2017). Molecular basis of ancestral vertebrate electroreception. Nature *543*, 391–396.
24. Baker, C.V.H., and Modrell, M.S. (2018). Insights into electroreceptor development and evolution from molecular comparisons with hair cells. Integr. Comp. Biol. *58*, 329–340.
25. Hafidi, A., Beurg, M., and Dulon, D. (2005). Localization and developmental expression of BK channels in mammalian cochlear hair cells. Neuroscience *130*, 475–484.
26. Roux, I., Safieddine, S., Nouvian, R., Grati, M., Simmler, M.C., Bahloul, A., Perfettini, I., Le Gall, M., Rostaing, P., Hamard, G., et al. (2006). Otoferlin, defective in a human deafness form, is essential for exocytosis at the auditory ribbon synapse. Cell *127*, 277–289.
27. Vincent, P.F., Bouleau, Y., Charpentier, G., Emptoz, A., Safieddine, S., Petit, C., and Dulon, D. (2017). Different $Ca_V1.3$ channel isoforms control distinct components of the synaptic vesicle cycle in auditory inner hair cells. J. Neurosci. *37*, 2960–2975.
28. Kollmar, R., Fak, J., Montgomery, L.G., and Hudspeth, A.J. (1997). Hair cell-specific splicing of mRNA for the alpha1D subunit of voltage-gated Ca^{2+} channels in the chicken's cochlea. Proc. Natl. Acad. Sci. USA *94*, 14889–14893.
29. Holt, C., Campbell, M., Keays, D.A., Edelman, N., Kapusta, A., Maclary, E., Domyan, E.T., Suh, A., Warren, W.C., Yandell, M., et al. (2018). Improved genome assembly and annotation for the rock pigeon (*Columba livia*). G3 (Bethesda) *8*, 1391–1398.
30. Modrell, M.S., Bemis, W.E., Northcutt, R.G., Davis, M.C., and Baker, C.V. (2011). Electrosensory ampullary organs are derived from lateral line placodes in bony fishes. Nat. Commun. *2*, 496.
31. Jørgensen, J.M. (2005). Morphology of electroreceptive sensory organs. In Electroreception, T.H. Bullock, C.D. Hopkins, A.N. Popper, and R.R. Fay, eds. (Springer), pp. 47–67.
32. Baker, C.V., Modrell, M.S., and Gillis, J.A. (2013). The evolution and development of vertebrate lateral line electroreceptors. J. Exp. Biol. *216*, 2515–2522.
33. Trincker, D. (1957). [Structural potentials in the semicircular canal system of guinea pigs & their changes in experimental deviations of the cupula]. Pflugers Arch. Gesamte Physiol. Menschen Tiere *264*, 351–382.
34. Cohen, M.M. (1981). Intersensory Perception and Sensory Integration (Plenum Press).
35. Keeton, W.T. (1971). Magnets interfere with pigeon homing. Proc. Natl. Acad. Sci. USA *68*, 102–106.
36. Ioalè, P. (2000). Pigeon orientation: effects of the application of magnets under overcast skies. Naturwissenschaften *87*, 232–235.
37. Moore, B.R. (1988). Magnetic fields and orientation in homing pigeons: experiments of the late W. T. Keeton. Proc. Natl. Acad. Sci. USA *85*, 4907–4909.
38. Mouritsen, H., Huyvaert, K.P., Frost, B.J., and Anderson, D.J. (2003). Waved albatrosses can navigate with strong magnets attached to their head. J. Exp. Biol. *206*, 4155–4166.
39. Bonadonna, F., Bajzak, C., Benhamou, S., Igloi, K., Jouventin, P., Lipp, H.P., and Dell'Omo, G. (2005). Orientation in the wandering albatross: interfering with magnetic perception does not affect orientation performance. Proc. Biol. Sci. *272*, 489–495.
40. Kirschvink, J.L. (1992). Uniform magnetic fields and double-wrapped coil systems: improved techniques for the design of bioelectromagnetic experiments. Bioelectromagnetics *13*, 401–411.
41. R Development Core Team (2013). R: a language and environment for statistical computing (R Foundation for Statistical Computing).
42. Schindelin, J., Arganda-Carreras, I., Frise, E., Kaynig, V., Longair, M., Pietzsch, T., Preibisch, S., Rueden, C., Saalfeld, S., Schmid, B., et al. (2012). Fiji: an open-source platform for biological-image analysis. Nat. Methods *9*, 676–682.

STAR★METHODS

KEY RESOURCES TABLE

REAGENT or RESOURCE	SOURCE	IDENTIFIER
Antibodies		
Rabbit anti C-FOS	Santa Cruz	Cat#sc-25; RRID: AB_2231996
Rabbit anti CACNA1D	Alomone labs	Cat#ACC-005
Mouse anti MaxiKalpha	Santa Cruz	Cat#sc-374142; RRID: AB_10919141
Mouse anti acetylated Tubulin	Sigma Aldrich	Cat#T6793; RRID: AB_477585
Goat anti Otoferlin	Santa Cruz	Cat#sc-50159; RRID: AB_785002
Mouse anti Syntaxin-1 (SP6)	Santa Cruz	Cat#sc-20036; RRID: AB_628316
Donkey anti rabbit Alexa Fluor-488	Thermo Fischer	Cat#A-21206; RRID: AB_2535792
Donkey anti goat Alexa Fluor-568	Thermo Fischer	Cat#A-11057; RRID: AB_2534104
Donkey anti mouse Alexa Fluor-647	Thermo Fischer	Cat#A-31571; RRID: AB_162542
Chemicals, Peptides, and Recombinant Proteins		
Paraformaldehyde	Sigma Aldrich	S9378
Diaminobenzidine	Sigma Aldrich	D5905
Hydrogen peroxide	Merck	822287
D-mannitol	Sigma Aldrich	M4125
Neg-50 frozen section medium	Thermo Fischer	6502
Triton X-100	Sigma Aldrich	X100
Donkey serum	Abcam	ab7475
Fluorescent Mounting Medium	Dako	S302380
AluI	NEB	R0137S
Critical Commercial Assays		
Antigen Unmasking Solution	Vector Laboratories	H-3301
VECTASTAIN Elite ABC HRP Kit	Vector Laboratories	PK-6100
RNeasy mini kit	Quiagen	74104
Quantitect reverse transcription kit	Quiagen	205313
Phusion Hot Start Flex NA polymerase	NEB	M0535S
TOPO-TA Cloning Kit	Thermo Fischer	45-0030
Oligonucleotides		
CACNA1D_27F: CAGGAGTGTTCACTGTTGA	This paper	N/A
CACNA1D_29R: TATTGGCAGCATAGTAGACGT	This paper	N/A
KCNMA1_8F: CAGCCACTAACGTATTGG	This paper	N/A
KCNMA1_10R: TCGCTACGTGCCAG	This paper	N/A
Software and Algorithms		
Pannoramic Viewer, Version 1.15.4	3D Histech	N/A
Definiens Architect XD	Definiens Software	N/A
R	[40]	N/A
iTOL v4	https://itol.embl.de/	N/A
Prism software for graphs and statistical analysis, version 7	GraphPad Software	N/A
FIJI	[8]	N/A
Other		
Magnetically shielded room	Magnetic shields	N/A
3D Helmholtz coil system	Serviciencia	BH1300-3-A
DC power source	Aim TTi	CPX400DP
Slide scanner	3D Histech	Pannoramic 250 FlashIII
Nanovoltmeter	Keithley Nanovoltmeter	2182A

(*Continued on next page*)

Continued

REAGENT or RESOURCE	SOURCE	IDENTIFIER
Cryostat	Thermo Fischer	MICROM HM 560
Laser scanning confocal microscope	Zeiss	LSM780
Tissue lyser II	Quiagen	128091236

LEAD CONTACT AND MATERIALS AVAILABILITY

Further information and requests for reagents may be directed to and will be fulfilled by the lead contact, David A. Keays (keays@imp.ac.at). This study did not generate new unique reagents.

EXPERIMENTAL MODEL AND SUBJECT DETAILS

Male and female adult rock pigeons (*Columba livia*) from our Austrian cohort were maintained on a 12:12 light-dark cycle at 25°C in a custom-built aviary. For the magnetic stimulation assay, 45 experimental birds were used. Six animals were used for tissue cDNA preparations and 6 used for immunohistochemical experiments. Animals were housed and experimental procedures were performed in accordance with an existing ethical framework (GZ: 214635/2015/20) granted by the City of Vienna (Magistratsabteilung 58).

METHOD DETAILS

Magnetically shielded room and magnetic coils

The experiments were performed inside a 4.4 m long, 2.9 m wide and 2.3 m high room which was shielded against oscillating electromagnetic fields by a 5 mm thick aluminum layer and against static magnetic fields by a 1 mm thick layer of mu-metal (Figure 1A) (Magnetic Shielding, UK). The ambient magnetic field intensity inside the room was attenuated to 0.3 μT and maximum radio frequency intensities between 0.5 to 5 MHz were below 0.01 nT. Magnetic fields were generated using a double-wrapped, custom-built 3D-Helmholtz coil system (Serviciencia, S. L) situated in the center of the shielded room (Figure 1B). Double wrapped coils permit the generation of magnetic stimuli when current flows in parallel through the coils. In contrast in the control condition current flows antiparallel, generating the same heat and vibration to the experimental situation but no magnetic stimulus [40]. The diameters of the coils were: 1,310 mm (x axis), 1,254 mm (y axis), and 1,200 mm (z axis). The coils were driven by DC power sources (TTI CPX400DP) and a computer situated outside the magnetically shielded room. All cables leading into the room were filtered for radio frequencies.

Subjects and Stimulations

Adult pigeons (*Columba livia*) underwent a surgical procedure to glue (UHU, 37420) a 3D printed polylaurinlactam non-magnetic head-stud to the pigeon skull to restrict head movement during the experiment (Figures 1C and 1D). The animals were habituated to our shielded room, the body harness, and the head fixation apparatus for 30 minutes on 3 consecutive days prior to the experiment. Pigeons were then exposed to a rotating magnetic field of 150 μT (n = 22) or to a zero magnetic field (n = 23). The magnetic field applied replicated that employed by Wu and Dickman. Briefly, it consisted of 360° rotations with 6° steps every 2 s (120 s in total). After each rotation the plane was shifted by 15° and the procedure repeated. This occurred 12 times (a full 360°) around the x axis and then for the y- and z-axes. For the zero-magnetic field control the same protocol was used but currents ran antiparallel through the double-wrapped coils, producing a null magnetic field. Exposure to magnetic stimuli lasted for 72 minutes and was performed either in darkness (n = 30) or under white light (400-700 nm, intensity of ~760 Lux, n = 15). The experimenters were blind to the stimulation conditions at all times. At the completion of the experiment birds were immediately sacrificed and perfused intracardially with 200 ml of 4% PFA in PBS (Sigma Aldrich, 158127). The brains were dissected, postfixed in 4% PFA for 18 hours at 4°C, dehydrated in 30% sucrose (Sigma Aldrich, S9378) for 3 days at 4°C and sectioned in the coronal plane on a sledge microtome (40 μm).

Immunohistochemistry on brain sections

The vestibular nuclei were identified using a pigeon brain atlas [8]. Three sections between stereotaxic coordinates P 2.25 and P 2.50 were selected for analysis. Sections were mounted on glass slides, dried for 2 days at room temperature followed by 3 washes in PBS (5 minutes each). Antigen retrieval was then performed in a water bath using antigen unmasking solution heated up to 90°C over 1 hour (Vector Laboratories, H-3301). After another washing step (3x5 minutes in PBS), slides were incubated with the C-FOS antibody (1:1500, Santa Cruz, sc-253) in 4% milk/0.3% Triton X-100/PBS for 16 hours at room temperature. Slides were washed 3x5 minutes in PBS, incubated with the secondary antibody (1:1000, anti-rabbit, Vectastain Elite ABC HRP Kit, PK-6100, Vector Laboratories) for 2 hours at room temperature, followed by another washing step and incubation with the AB reagent (Vectastain Elite ABC HRP Kit, PK-6100, Vector Laboratories) for 1 hour. After another round of washing, slides were incubated in 0.06% Diaminobenzidine (Sigma Aldrich, D5905) in PBS supplemented with 0.08% H_2O_2 (Merck, 822287) for 1 minute, followed by 3x5 minute washes in PBS, dehydration in serial dilutions of ethanol and coverslipping. All sections of all birds underwent the staining procedure at the same time to minimize variation in background staining.

Counting and statistical analysis

Slides were scanned on a slide scanner with a 20x objective (Pannoramic 250 Flash III, 3DHistech) and the vestibular nuclei manually segmented (6 bilateral segments from 3 sections) using Pannoramic Viewer (Pannoramic Viewer 1.15.4, 3DHistech). Segments were exported as TIFF files for further analysis. Automated identification and counting of C-FOS positive nuclei was performed by custom made rule-sets using a machine-learning algorithm embedded in the Definiens Architect software (Definiens Architect XD, Definiens Software). The number of C-FOS positive cells per mm^2 was calculated. To analyze the effects of the magnetic stimulation on neuronal activation we performed two-way ANOVAs, using the factors: magnetic treatment, light condition and their interaction. Prior to execution of this statistical test we checked all four groups using the Shapiro-Wilk normality test and found that all groups did not differ from normality. We used the software R [41] for all statistical analyses. Figures were generated using Graphpad Prism (Prism 7 for Mac OS X).

Generation of cell density maps

The mean distance between C-FOS positive nuclei was used to generate heatmaps. Specifically, we employed the following algorithm: $I = 1/\sqrt{(2*MDo+\sum MD)/(2+N)}$, where I in the intensity, MDo is the mean distance to boarder of a neighboring positive cell, MD is the sum of the mean distances, and N is the number of neighboring cells. Heatmaps were averaged for each treatment group by registration onto a reference template. Section borders were corrected for mapping errors. From averaged heatmaps, a differential C-FOS positive cell density map was generated comparing control and magnetic conditions. All image-processing steps were performed using custom-written macros in Fiji [42].

Modeling of electromagnetic induction in an artificial pigeon semicircular canal

Polyurethane tubing (0.8 cm inner diameter, 1.2 cm outer diameter) was used to build a replica of a pigeon semicircular canal with a diameter of 21 cm and a circumference of 69 cm (Figure 3A). The tubing was filled with artificial pigeon endolymph consisting of 141.35 mM potassium, 0.23 mM calcium and 141.81 mM chloride in monoQ H_2O [17]. The osmolarity was adjusted to 293 mOsm/L with D-mannitol (Sigma Aldrich, M4125) and pH was adjusted to 7.4. Both ends of the loop were closed with gold plated electrodes and connected to a nanovoltmeter (Keithley Nanovoltmeter Model 2182A). The tubing was positioned in the center of our Helmholtz coil system and exposed to a rotating magnetic field of 150 μT around the vertical axis (6° step changes every 2 s, 120 s in total). The induced voltage in the artificial semicircular canal was measured using the nanovoltmeter. The voltage measurement was performed every 10 ms with signal integration between two measurement points to enhance the signal-to-noise ratio. Afterward, the recorded signal was filtered with a digital Butterworth filter (library functions *butter* and *filtfilt* part of the python package *signal* in *scipy*; the used parameters were as follow: order of the filter = 5, critical frequency = 0.15) to reduce the low frequency background from the measurement system.

Physical calculations

To estimate the diameter of each semicircular canal we measured from the center of the bony canal to the vestibule (n = 3 birds), drawing on previously published CT reconstructions of the pigeon inner ear [18]. The induced voltage, u, is defined as $u = -(\partial\Phi_B/\partial t)$, where Φ_B is the magnetic flux. Using the geometry of the set-up this expression can be written as $u = (\partial B/\partial t)\cdot A$, with B the applied magnetic field and A the area enclosed by a semicircular canal. The electric field, E, in the semicircular canal is calculated with $E = (u/2\pi r)$, where r is the radius of the semicircular canal and u the measured induced voltage. We then applied a scaling factor which was calculated by dividing the radius of one semicircular canal by the radius of the artificial inner ear. To estimate the electric field, E_n, generated by natural head movement we employed the following equation: $E_n = B_0 \cdot \pi f \cdot r$, where r is the radius of the semicircular canal, B_0 is the Earth's field, and f is the frequency of head scanning.

Immunohistochemistry on semicircular canal sections

Pigeon temporal bones containing intact inner ears were fixed overnight in 4% PFA. Following a wash in PBS, ampullae in the membranous labyrinth were dissected under a stereomicroscope. Tissues were dehydrated in 30% sucrose/PBS overnight, embedded in Neg-50 Frozen Section Medium (Thermo Fisher, 6502) and sectioned (10 μm) on a cryostat (Thermo Fisher, MICROM HM 560). Slides were dried at RT for at least 1 h prior to staining, washed in 3 × 5 min in PBS, and exposed to heat-based antigen retrieval (Vector Laboratories, H-3301). After a 30 min cooling period and 3 × 5 min washes in PBS, slides were incubated overnight with antibodies diluted in 0.3% Triton X-100/PBS (Sigma Aldrich, X100) with 2% donkey serum (Abcam, ab7475). The following concentrations were used: 1:300 $Ca_v1.3$ (Alomone labs, ACC-005), 1:300 BK (Santa Cruz, sc-374142), 1:500 acetylated Tubulin (Sigma-Aldrich, T6793), 1:300 Otoferlin (Santa Cruz, sc-50159), 1:500 Syntaxin 1 (Santa Cruz, sc-20036). The next day, slides were washed 3 x in PBS for 5 min and incubated with donkey anti-rabbit Alexa Fluor-488 (Thermo Fisher, A-21206), donkey anti-goat Alexa Fluor-568 (Thermo Fisher, A-21206), and donkey anti-mouse Alexa Fluor-647 (Thermo Fisher, A-31571), each diluted 1:500, for 1 h at 4c°C. After counterstaining with DAPI and 3 × 5 min washes in PBS, slides were mounted with Fluorescent Mounting Medium (Dako, S302380). Images were acquired using a laser scanning confocal microscope (Zeiss, LSM780), and processed in ImageJ [42].

PCR analysis of $Ca_v1.3$ (CACNA1D) splice isoforms

Tissue samples (brain, pineal gland, retina, cochlea, vestibular epithelia, respiratory cochae, skin, heart, muscle, liver, and spleen) were collected from adult pigeons (*Columba livia*), snap-frozen in liquid nitrogen, and mechanically homogenized with a tissue lyser

(QIAGEN Tissue Lyser II, 128091236). For the vestibular epithelia the ampullae, lagena, utricle and saccule were pooled. Total RNA was extracted from tissue lysates using the RNeasy mini kit (QIAGEN, 74104) and reverse transcribed with a Quantitect Reverse Transcription Kit in accordance with the manufacturers' instructions (QIAGEN, 205313). The cDNA libraries were diluted to a working concentration of 1:100 and stored at −20°C. Polymerase chain reaction (PCR) primers flanking exon 28a were designed based on available genomic resources. The primer sequences were F: CAGGAGTGTTCACTGTTGA; and R: TATTGGCAGCATAGTA GACGT. PCR amplification of the tissue cDNA libraries was performed with the Phusion Hot Start Flex DNA polymerase (NEB, M0535S). PCR products were analyzed by agarose gel electrophoresis (4%).

PCR analysis of BK (KCNMA1) splice isoforms

To determine the tissue specific expression of different BK (KCNMA1) splice isoforms we designed an assay that relies on PCR amplification of a 239 bp fragment that spans exons 8 to 10 followed by a restriction digest. The primer sequences were F: CAGCCAC TAACGTATTGG; and R: TCGCTACGTGCCAG. We amplified the aforementioned cDNA libraries using Phusion Hot Start Flex DNA polymerase (NEB, M0535S). A restriction digest was then performed using AluI (NEB, R0137S) which discriminates between exon 9a (SI isoform; TTT-GCC-AG^C-TAC) and exon 9b (RA isoform; TTT-GCT-CGC-TAC; no target). PCR products were digested following gel purification for one hour at 37°C and analyzed by agarose gel electrophoresis (2%). Exon 9a and 9b isoforms amplicons from vestibular tissue were TA-cloned into pCR4-TOPO (Thermo Fischer, 45-0030) in accordance with the manufacturer's protocol and their sequence confirmed.

Phylogenetic analysis of $Ca_v1.3$ (CACNA1D) and BK (KCNMA1) splice isoforms

We explored the taxonomic distribution of the 10 amino acid insertion in the pore-forming alpha1D subunit of $Ca_v1.3$ (CACNA1D) and RA isoform in the BK (KCNMA1) channel using a sequence-similarity based strategy. To identify CACNA1D homologs containing the KKER insertion we performed a BLASTp search with a 50 amino acid long segment of pigeon $Ca_V1.3$ (centered around the insertion) against the NCBI non-redundant protein database (NP_990365.1:1264-1313; BLASTP v2.8.1+; limited to the top 10000 target sequences). Only sequences with similarity in 5 out of the 10 amino acid positions were kept. In the case of the BK channel a BLASTp search was performed with the RA isoform ± 20 flanking amino acids against the NCBI non-redundant protein database. We derived species phylogenetic trees using NCBI's Common Tree and iTOL v4.

QUANTIFICATION AND STATISTICAL ANALYSIS

To analyze the effects of the magnetic stimulation on neuronal activation we performed two-way ANOVAs, using the factors: magnetic treatment, light condition and their interaction. Prior to execution of this statistical test we checked all four groups using the Shapiro-Wilk normality test and found that all groups did not differ from normality. We used the software R [41] for all statistical analyses. One animal was excluded from analysis because of methodological problems (sections detached from the slide and could not be further analyzed). The exact sample sizes, means, and standard deviations can be found in the results section of the paper (one "n" is defined as one animal). We defined a significant result with $p < 0.05$ throughout the paper. The treatment conditions were randomized on each test day and the experimenters where blind to the applied treatments.

DATA AND CODE AVAILABILITY

The rule-sets used to quantify C-FOS positive cells in the current study have not been deposited in a public repository as they are embedded in the Definiens Architect software but the used parameters are available from the corresponding author on request.